Tech Science Press

Isolation of Thermally Stable Cellulose Nanocrystals from Spent Coffee Grounds via Phosphoric Acid Hydrolysis

Brody A. Frost and E. Johan Foster*

Virginia Tech, Department of Materials Science and Engineering, Macromolecules Innovation Institute, 117 Surge, Virginia Tech, Blacksburg, VA 24061, USA
*Corresponding Author: E. Johan Foster. Email: johanf@vt.edu

Abstract: As the world's population exponentially grows, so does the need for the production of food, with cereal production growing annually from an estimated 1.0 billion to 2.5 billion tons within the last few decades. This rapid growth in food production results in an ever increasing amount of agricultural wastes, of which already occupies nearly 50% of the total landfill area. For example, is the billions of dry tons of cellulose-containing spent coffee grounds disposed in landfills annually. This paper seeks to provide a method for isolating cellulose nanocrystals (CNCs) from spent coffee grounds, in order to recycle and utilize the cellulosic waste material which would otherwise have no applications. CNCs have already been shown to have vast applications in the polymer engineering field, mainly utilized for their high strength to weight ratio for reinforcement of polymer-based nanocomposites. A successful method of purifying and hydrolyzing the spent coffee grounds in order to isolate usable CNCs was established. The CNCs were then characterized using current techniques to determine important chemical and physical properties. A few crucial properties determined were aspect ratio of 12 ± 3, crystallinity of 74.2%, surface charge density of (48.4 ± 6.2) mM/kg cellulose, and the ability to successfully reinforce a polymer based nanocomposite. These characteristics compare well to other literature data and common commercial sources of CNCs.

Keywords: Cellulose nanocrystals; phosphoric acid hydrolysis; agricultural waste; industrial waste; spent coffee grounds; polymeric nanocomposites; renewable cellulosic materials

1 Introduction

Cellulose is one of the most abundant natural, renewable, and biodegradable polymers on Earth, and can be obtained from various sources including bacteria, forestry, and agricultural wastes (agro-wastes) [1, 2]. It is mainly found in plant cell walls, lending its physical strength to the structure of the plant due to its strong, tightly packed structure [1, 2]. Its linear unbranched homopolysaccharide structure comprising of 1-4 β linked glycosidic bonds, as well as the hydrogen bonding of the C2 and C6 hydroxyl groups between cellulose molecules, allows for the formation of crystalline regions throughout the cellulose chains [3, 4]. These crystalline regions can be isolated by multiple techniques, with acid hydrolysis being the most

common. This technique utilizes concentrated acids to hydrolyze the amorphous region of cellulose, resulting in the isolation of the crystalline regions [5, 6]. The most common and industrial/commercial acid hydrolysis procedure utilizes sulfuric acid due to the ease of use and established protocols, although other acids have been employed as well, such as phosphoric acid and hydrochloric acid [5, 7, 8]. These isolated crystalline nanomaterials, better known as cellulose nanocrystals (CNCs) and cellulose nanofibrils (CNFs), have been proven to have significant impacts on the field of polymer science [5-6].

CNCs and CNFs have been well explored in the past few decades, with ever increasing methods of isolation and applications [5, 6]. As previously mentioned, multiple different acids can be used to hydrolyze cellulose, which create different functionalizations on the surfaces of CNCs (i.e., sulfate, phosphate, and hydroxyl groups, among others), and lead to varying chemical and physical properties [8-10]. Although their structures are relatively the same, consisting of rod-like shapes ranging from 100 nm-1000 nm in length and 5 nm-20 nm in width, the varying functionalizations of the surface change properties such as dispersion in solvents, thermal stability, biocompatibility, and crystallinity or stiffness [8, 11, 12]. Their many unique properties allow for usage in a variety of applications, but are most known for their incredible strength to weight ratio for reinforcing nanocomposites, sustainability, and impact on environmentally friendly and biodegradable solutions in industry [5, 6, 13]. The use of CNCs as a reinforcing agent in polymer nanocomposites, has seen a drastic rise in the last few years, leading to many new applications in many different fields [14-17]. When CNCs are added into a polymer, they have the ability to not only change the mechanically behavior, but also to increase properties such as water absorption in hydrophilic polymers, produce repeatable actuation, and promote particle adsorption and cell growth and viability [5, 6, 11, 12, 18, 19]. Some applications in particular that have been explored are reinforcement in polyethylene, polyester, and polyurethane nanocomposites for use in automotive, textile, and biomedical industries [11, 12, 14, 20-22], as well as use in optical [23], electronic [24], and stimuli responsive materials [25-29], and airborne filtration systems [30]. The usefulness of CNCs and CNFs have given rise to a growing market for cellulose nanomaterials, with nearly 10,000 tons being produced per year and used in high-end industrial products as reported by Future Market Inc. (2019) [13].

As previously mentioned, trillions of tons of cellulose are produced globally annually, making it an almost inexhaustible feed source. For example, over six billion cups of coffee are consumed daily, leading to enormous amounts of raw cellulosic material just from spent coffee grounds [1, 4, 31, 32]. However, much of the cellulose is discarded as waste into landfills to eventually biodegrade [33]. One of the biggest impacts on landfill occupation has been from the agro-wastes produced by crop harvesting, food industry waste, and textile industry waste [33-35]. Due to the overwhelming amount of cellulosic materials discarded every year, extracting useful materials from various waste sources could potentially decrease landfill area, while leading to useful applications of the extracted material [33, 34]. For example, corn stover [36, 37], rice husks [38], cotton [39], and sugarcane bagasse [40] have had extensive research performed on the extraction of cellulose nanomaterials utilizing acid hydrolysis. However, there remains many other cellulose sources that have yet to be studied, such as spent coffee grounds, of which this research will focus.

Although research has been successful with isolating CNCs from coffee husks and coffee silver skins, spent coffee grounds have yet to be researched [41, 42]. This report seeks to provide a method of CNC extraction from spent coffee grounds utilizing adaptations of known purifying and hydrolyzing procedures [8, 43]. Once extracted, the CNCs are thoroughly characterized by current techniques and compared to literature to determine the viability of spent coffee grounds as a source for isolation of useful CNCs [9]. One of the most important factor of success will be determining the new CNC's ability to mechanical reinforce a polymer. The greater the mechanical reinforcement, the greater the ability to fine tune polymer nanocomposites, which will increase the variety of potential applications, as mentioned above [11, 12, 21, 44]. If proven successful, this research could provide an alternative way to recycle and reuse an otherwise useless waste material.

2 Experimental Methods

2.1 Materials

Café Bustello very fine coffee grounds were purchased from Food Lion in Blacksburg, Virginia. All chemicals including toluene, ethanol, 85% v/v phosphoric acid, sodium hydroxide pellets, acetic acid, N, N-dimethylformamide (DMF), dimethyl sulfoxide (DMSO), tetrahydrofuran (THF), and bovine serum albumin (BSA) were purchased from Sigma-Aldrich. McKesson 3% topical hydrogen peroxide was purchased from Amazon.com. Nanovan stain consisting of a suspension of vanadium particles in water was purchased from Nanoprobes. Texin RxT85A thermoplastic polyurethane (PU) was purchased from Covestro. Commercial cellulose nanocrystals (CNCs) were purchased from the University of Maine Nanocellulose Facility.

2.2 Purification and Bleaching of Cellulose

Café Bustello coffee grounds were run through a Keurig K series coffee machine to make a normal 8 oz. cup of coffee. It should be noted that the coffee grounds going through the heated water of the Keurig (roughly 90°C) experienced no thermal decomposition. As well, the initial roasting of the coffee beans to enhance flavor happens between 180-240°C, therefore the cellulose within coffee grounds underwent no prior thermal decomposition before use [45]. The spent coffee grounds were then left out to dry overnight before starting the cellulose extraction process. The relative composition of the spent coffee grounds after drying and before purification is shown below in Tab. 1 [31, 32, 46].

Table 1: Relative chemical composition of spent coffee grounds, adapted from Mussatto et al. (2011) and Ballesteros et al. (2014) [31, 32, 46]

Chemical Component	Dry Weight (g/100 g)
Cellulose	8-10
Hemicellulose	36-39
Lignin	23
Protein	13-17
Fat	2-3
Acetyl Groups	2
Ashes	1-2
Other (Not Specified)	4-15

The following purification and bleaching procedure was adapted from Marett et al. (2017) and Mueller et al. (2014) [43, 47]. Approximately 40 g of dried spent coffee grounds were measured out and purified utilizing a Soxhlet extraction procedure with a 1000 mL mixture of 1/3 ethanol and 2/3 toluene by volume. The solvent mixture was added to a round bottom flask under the extractor and placed into a silicone oil bath at 120°C to be boiled overnight, ensuring a significant amount of time to remove soluble monomers such as lipids. After roughly 24 h of extraction, the coffee grounds were removed and left to dry overnight.

Following the Soxhlet extraction, a 1 M sodium hydroxide bath was used to remove the soluble hemicellulose. The base wash was created by mixing 120 g of sodium hydroxide pellets with 3000 mL of deionized (DI) water and heating to 70°C while continuously stirring until all of the pellets were dissolved. The extracted material was added to the solution for 4 h and subsequently separated via

vacuum filtration. The resulting material was then washed with DI water until the liquid remained clear, approximately six times. This entire procedure was repeated one more time due to the extensive quantities of hemicellulose.

Immediately following the base washes, the almost-pure cellulose was added to a hydrogen peroxide/ acetic acid solution in order to remove the remaining non-cellulosic components including lignin. The wash comprised of 1440 mL of 3% hydrogen peroxide, 60 mL of acetic acid, and 1500 mL of DI water (48 v/v, 2 v/v, and 50 v/v of each component, respectively) and was heated to 60°C while stirring constantly. The cellulose was added to the wash for 4 h before separation via vacuum filtration. The resulting cellulose was then washed with DI water until the liquid remained clear, approximately four times. Again, this entire procedure was repeated one more time due to the extensive quantities of the remaining non-cellulosic components.

2.3 Acid Hydrolysis of Cellulose

The following phosphoric acid hydrolysis procedure was adapted from Espinosa et al. [8]. Two grams of the purified cellulose was added to 100 mL of DI water and cooled in an ice bath for 15 min. Phosphoric acid was slowly added dropwise via a dripping funnel, while maintaining a solution temperature of below 20°C, until a phosphoric acid concentration of 10.7 M was achieved (approximately 292 mL). After the addition of the acid was complete, the solution was placed in a silicone oil bath preheated to 100°C and stirred for a predefined time of 2 h. After the completion of the reaction, the solution was immediately moved into an ice bath until room temperature was reached. The phosphorylated CNCs (p-CNCs) were separated from the supernatant by centrifugation at 10000 rpm for 10 min. The separated supernatant was decanted, replaced by an equal amount of DI water, and centrifuged again. This step was repeated until the supernatant remained clear (approximately five times). The p-CNCs dispersion was dialyzed against DI water for 7 days, replacing the water every day, until a neutral pH of 7 was reached. The yield of p-CNCs was approximately 10%, however, it should be noted that the yield was highly dependent on the small content of cellulose residing in the raw spent coffee grounds [31, 32, 46]. To dry the p-CNCs, the suspension underwent a solvent exchanged into acetone by replacing 2/3 of the aqueous suspension with equal parts of acetone using the previously described sonication and centrifugation techniques. This process was repeated roughly 4 to 5 times to ensure complete exchange. Once the p-CNCs were exchanged into acetone, the suspension was poured into a Teflon petri dish and dried on a hotplate overnight. The subsequently dried p-CNCs were then used in the following characterization techniques, *Sections 2.4-2.11*, and redispersed into respective solvents as needed.

2.4 Microscopy

2.4.1 Scanning Electron Microscopy

SEM samples were prepped by dispersing p-CNCs in DMF with a concentration of 0.1 mg/mL, and sonicating at 110 W and frequency of 40 kHz with a Branson M2800 ultrasonic bath for 1 h. A droplet of the dispersion was then placed onto a silicon wafer attached to an aluminum SEM stand, and left in a desiccator to dry overnight. Each sample was sputter coated with 5 nm of iridium using a Leica ACE600 Sputter to prevent charge buildup, and imaged using a LEO 1550 field-emission SEM at 5 kV.

2.4.2 Transmission Electron Microscopy

TEM samples were prepped by dispersing p-CNCs in DI water with a concentration of 0.01 mg/mL, and sonicating at an amplitude of 40 with a 20 kHz Q55 Qsonica horn sonicator for 10 mins. Next a solution of BSA in DI waster was created at a concentration of 0.2 mg/mL, and mixed with the p-CNC dispersion in a 1:1 ratio. The subsequent mixture was then sonicated further at 110 W and frequency of 40 kHz with a Branson M2800 ultrasonic bath for 1 h. A droplet of the mixture was placed onto a copper TEM grid and left for 1 min to ensure attachment of p-CNCs. A drop of NanoVan stain was then added to the TEM grid

for 30 s, before being quickly submerged in a beaker of DI water to remove any excess materials. The grid was left in a desiccator to dry overnight. Imaging was performed using a JEOL 2100 TEM.

2.5 Energy-dispersive X-ray Spectroscopy

EDS samples were prepped similarly to the SEM samples, however instead of dispersing in DMF, the p-CNCs were dispersed in DI water with a concentration of 10 mg/mL. The dispersion was sonicated at 110 W and frequency of 40 kHz with a Branson M2800 ultrasonic bath for 1 h. A drop of the dispersion was placed on a silicon wafer and left in a desiccator to dry overnight. As well, phosphorus has a relatively similar signal as iridium, therefore the samples were sputter coated with 5 nm of gold-palladium. Analysis was performed using a LEO 1550 field-emission SEM at 10 kV.

2.6 X-ray Photoelectron Spectroscopy

XPS samples were prepped similarly to the EDS samples, however a concentration of 1.0 mg/mL was used. The dispersion was sonicated at 110 W and frequency of 40 kHz with a Branson M2800 ultrasonic bath for 1 h. A drop of the dispersion was placed on a silicon wafer and left in a desiccator to dry overnight. The samples were not sputter coated prior, and analysis was performed using a PHI Quantera SXM-03.

2.7 Conductometric Titration

Conductometric titration was performed following a known protocol by Foster et al. 0.15 g of p-CNCs were dispersed in 300 mL of DI water and sonicated in an ultrasonic bath for 1 h. 5 mL of 0.5 M NaCl solution and 0.02 M HCl solution were added to the dispersion prior to titrating [9]. Titration was carried out by a Metrohm 905 Titrando automatic titrator dosing 0.05 mL of 0.02 NaOH solution per data point using an Metrohm 800 Dosino automatic doser, and measuring conductivity and pH with a Metrohm 856 conductivity module. Due to the addition of the NaCl, a calculated conductivity was used instead of the measured conductivity, following the equation used in Foster et al. [9]. The data was plotted and analyzed using Excel, and surface charge density calculated using an adapted protocol and equation by Espinosa et al. [8].

2.8 X-ray Powder Diffraction

XRD was performed on dry p-CNCs in powder form using a Panalytical X'Pert powder XRD system. A CuKα radiation source was used at 45 kV and 30 mA, and scattered radiation was detected in the range of $2\theta = 0°\text{-}50°$. Percent crystallinity was determined using the peak deconvolution method similar to that of Zhang et al. [48].

2.9 Thermogravimetric Analysis

TGA was performed on dry p-CNCs in powder form using a TA Instruments TGA Q500 thermal analyzer. 10 mg of p-CNCs were measured into a platinum TGA pan, and heated from 25°C to 500°C at a rate of 10°C/min. The decomposition temperature was determined by the loss of 5 wt% after the residual water had been removed from the sample.

2.10 Dispersability and Dynamic Light Scattering

The dried p-CNCs were dispersed in DI water, DMSO, DMF, and THF, decreasing in polarity, with a concentration 10 mg/mL. Each dispersion was sonicated using a 20 kHz Q55 Qsonica horn sonicator at an amplitude of 40 for 10 mins, followed by further sonication in an ultrasonic bath for 1 h. The dispersions were lined up in order of decreasing polarity and imaged immediately after sonication, and 1 h, 1 d, and 10 d post-sonication.

DLS samples were prepped by dispersing p-CNCs into DMF at a concentration of 0.01 mg/mL. The dispersion was sonicated using the same protocol mentioned above for dispersibility studies. The dispersions were then transferred to a quartz cuvette, and analyzed using a Malvern Zetasizer Nano-ZS DLS instrument to determine relative particle size within a suspension.

2.11 Mechanical Reinforcement

Three different compositions of composites were fabricated for mechanical reinforcement testing; neat PU, 10 w/w commercial CNCs in PU, and 10 w/w p-CNCs in PU, following an adapted procedure from Frost and Foster [21]. The CNCs were dispersed in DMF at a concentration of 10 mg/mL using the same sonication protocol discussed in dispersibility testing. The PU was dissolved in DMF at a concentration of 40 mg/mL using a hot plate at 140°C while stirring at 1000 rpm for 1 h or until all the PU pellets had dissolved. Once the CNC suspensions and PU solution were completely homogenous, they were mixed together in the ratios specified above. The combined mixture was placed in an oil bath at 140°C while stirring at 750 rpm until enough DMF was evaporated to increase viscosity (to the 'viscosity of molasses'). The viscous mixture was then transferred to a Teflon dish, set on a hot plate at 100°C, and left overnight to slowly evaporate the DMF. After drying overnight, the samples were put into a vacuum oven at 80°C and −27 in *Hg for 2 h or until all DMF was removed.

After complete removal of the solvent, each composition was hot pressed using a 3851-0 Carver Press at 140°C and 3 MPa of pressure for 5 min, using 0.9 mm–1.0 mm aluminum spacers to ensure uniformity of thickness throughout the film. Each pressed film was cut with a razor blade into five 1.0 cm wide ribbons for tension testing. Tension testing was performed utilizing a TA Q800 Dynamic Mechanical Analyzer (DMA) on five of each composite composition to determine the mechanical reinforcement properties of the composites. Each sample was tested using an isostatic force test with a force ramp rate of 3 N/min at 25°C until a maximum of 18 N was reached.

3 Results and Discussion

3.1 Isolation of p-CNCs from Spent Coffee Grounds

Due to the excessive amount of non-cellulosic components in the spent coffee grounds [31, 32, 46], the bleaching and purification process was adjusted to obtain a purer form of cellulose, yielding an off-white, slightly tan color. Of the 40.0 g of dried spent coffee grounds, a resulting 4.2 g yield was left after the bleaching and purification process, which correlates well to the previously reported amount of cellulose found in spent coffee grounds [31, 32, 46]. Following the extensive bleaching and purification process, extraction of p-CNCs from spent coffee grounds utilizing phosphoric acid hydrolysis proved successful. The cellulose was hydrolyzed using the same parameters as the procedure by Espinosa et al., however, an extra 30 min was added to the reaction time in order to fully hydrolyze the cellulose [8]. Phosphoric acid hydrolysis was chosen over the conventional sulfuric acid hydrolysis because of the difference in the resulting physical and chemical properties. Compared to traditional sulfated CNCs (s-CNCs), p-CNCs have a lower surface charge, decreasing dispersibility in many organic solvents, leading to more agglomerations within polymer composite systems. However, they have also been shown to have a higher thermal stability and biocompatibility (better cell growth and viability), which is crucial for multiple polymeric applications [5, 8, 11, 12]. The p-CNCs were successfully characterized, Tab. 2, following current analyzing techniques in literature and compared to other fabricated p-CNCs and current industrial CNCs [8, 9, 49, 50].

3.2 Microscopy – SEM and TEM

Both SEM and TEM were employed to determine whether p-CNCs were successfully obtained, and if so, to characterize the average aspect ratio. SEM imaging was performed first and compared to literature, to

Table 2: Physical and chemical properties of fabricated p-CNCs compared to fabricated p-CNCs in literature and commercial s-CNCs from UMaine and CelluForce [5, 8, 49, 50]

	Coffee p-CNCs	p-CNCs (Espinosa)[7]	p-CNCs (Vanderfleet)[8]	UMaine s-CNCs	CelluForce s-CNCs
Substituent content (phosphate and sulfate groups, respectively) (mM/kg cellulose)[1]	25.8 ± 9.6	3.95 ± 0.8	18.8 ± 3.3	1.06 ± 0.2	8.1 ± 0.05
Charge concentration (mM/kg cellulose)[2]	48.4 ± 6.2	10.8 ± 2.7	N/A	330 ± 15	255 ± 10
Carbon (%)[1]	58.5 ± 0.39	44.19 ± 0.15	N/A	~77	~77
Oxygen (%)[1]	40.5 ± 0.39	49.5 ± 0.08	N/A	~23	~23
Length (nm)[3]	199 ± 27	316 ± 127	326 ± 70	134 ± 52	183 ± 88
Diameter (nm)[3]	17 ± 4	31 ± 14	N/A	7 ± 2	6 ± 2
Aspect ratio[3]	12 ± 3	11 ± 1.5	N/A	19	31
Apparent crystallinity (%)[4]	74.2	81	95	85	89.9
Onset of thermal decomposition, $T_{d5\%}$ (°C)[5]	310	305	~300	~260	~263
Mechanical reinforcement tensile modulus at 10 wt% CNCs (MPa)[6]	58.6 ± 2.7	N/A	N/A	113.7 ± 9.7	N/A
Mechanical reinforcement yield stress at 10 wt% CNCs (MPa)[6]	2.6 ± 0.1	N/A	N/A	3.6 ± 0.0	N/A

[1] Determined by XPS (*Section 3.3*)
[2] Determined by conductometric titration (*Section 3.4*)
[3] Determined by TEM (*Section 3.2*)
[4] Determined by XRD (*Section 3.5*)
[5] Determined by TGA (*Section 3.6*)
[6] Determined by DMA (*Section 3.8*)
[7] Referenced from Espinosa et al. [8]
[8] Referenced from Vanderfleet et al. [49]

establish a preliminary presence of p-CNCs. The SEM images show the distinct rod-like shape of the p-CNCs, however, lack of a more diluted dispersion caused aggregation of the particles while drying. The resulting mat of material, shown in Fig. S1, is assumed to be the aggregated p-CNCs due to its common drying agglomeration, similar results found in literature [43, 51, 52].

TEM was subsequently conducted to determine the length, width, and aspect ratio of the p-CNCs, shown in Fig. 1, and compared to those found in literature [8, 11, 49]. It should be noted that although the images in Fig. 1 show a darkened region from the agglomeration of BSA protein around the p-CNCs, the measurements were not affected. ImageJ image measurement software was used to measure 15 individual p-CNCs from varying images, resulting in an average length of (199 ± 27) nm, average width of (17 ± 4) nm, and aspect ratio of 12 ± 3. Although the aspect ratio of the p-CNCs resides in the lower range of literature values [5, 6] (for reference, 10 for cotton and 67 for tunicates [12]), there should still be significant amount of mechanical reinforcement when introduced into a polymer matrix, discussed later in *Section 3.8*.
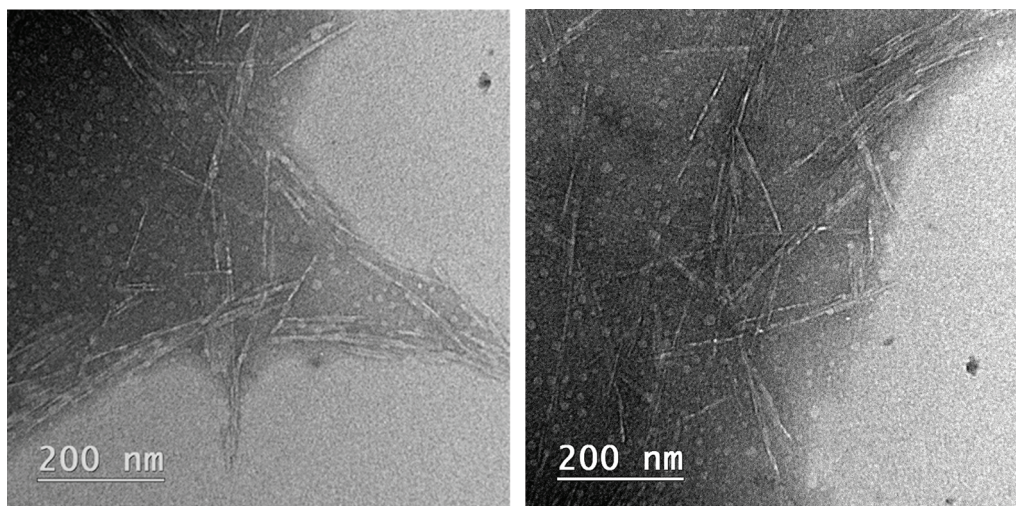
Figure 1: TEM images of isolated p-CNCs dispersed in a 1:1 mixture of 0.01 mg/mL p-CNCs in DI water and 0.2 mg/mL BSA solution. The BSA was shown to produce a darker halo around the p-CNCs due to agglomeration of the protein

3.3 Chemical Composition – EDS and XPS

EDS and XPS were conducted for elemental analysis of the p-CNCs, specifically for carbon, oxygen, and phosphate content. The elemental analysis resulted in a carbon content of (58.5 ± 0.39) wt%, and an oxygen content of (40.5 ± 0.39) wt%, which are typical values for cellulose and its derivatives [8]. The phosphate content was shown to be (0.08 ± 0.03) wt%, which was then converted to (25.83 ± 9.6) mM/kg cellulose for a more accurate comparison to literature values [8, 49]. It is typical to see a lower phosphate content for p-CNCs when compared to other functionalized CNCs, specifically sulfation of s-CNCs which ranges from 80 mM/kg cellulose-350 mM/kg cellulose [43, 49]. However, the phosphate content observed for the p-CNCs is much higher than expected when compared to other studies (i.e., 3.95 ± 0.8 mM/kg cellulose for Espinosa et al. and 8.2 mM/kg cellulose-44.5 mM/kg cellulose from Vanderfleet et al.) [8, 49]. Spent coffee grounds contain a certain wt% of phosphorus, and although it is assumed that all of the non-cellulosic materials were extracted during the bleaching and purification process, there is a potential chance for some of the phosphorus to remain, resulting in a higher phosphate content [31, 32, 46].

3.4 Surface Charge Density – Conductometric Titration

During acid hydrolysis, CNCs often become functionalized with associated groups of the acid being used, for example phosphate groups via phosphoric acid hydrolysis. Conductometric titration was employed to obtain the surface charge density of the functionalized p-CNCs, shown in Fig. S2. With the addition of phosphate substituents attached to the cellulose via ester bond, the surface charge should increase when compared to a blank titration. Utilizing adapted procedures from Foster et al. and Espinosa et al. [8, 9], surface charge density was calculated to be (48.4 ± 6.2) mM/kg cellulose. Although the surface charge is relatively high for p-CNCs compared to literature (10.8 ± 2.7 mM/kg cellulose by Espinosa et al.) [8], it correlates to the higher phosphate content of the spent coffee ground p-CNCs observed by EDS and XPS during elemental analysis [49]. The higher surface charge density will allow for easier dispersion in polar solvents such as water, DMSO, and DMF, however, will inherently lower the onset of thermal degradation, further discussed *Section 3.6 and 3.7*, respectively.

3.5 Crystallinity - XRD

XRD was performed to obtain the apparent crystallinity of the p-CNCs, shown in Fig. 2. The crystalline peaks occur at 2θ values of 16.5°, 20.5°, 22.5°, and 34.5°, which line up with the 10$\bar{1}$, 021, 002, and 040 planes, respectively, and indicative of cellulose type I [53]. It is common that an additional peak appears at 14.5° lining up with a 101 peak, when analyzing CNCs, however no peak occurred for the p-CNCs [53, 54]. This could indicate that not all of the amorphous region was hydrolyzed during the extraction process, leading to a slightly lower crystallinity. Under the assumption that the 101 and 10$\bar{1}$ peaks were the same intensity, a peak deconvolution method adapted from Zhang et al. (2014) was used to remove the amorphous material regions and calculate an apparent crystallinity of 74.2% [48]. The typical crystallinity of CNCs reported in literature ranges from 64% to 90%, with the majority residing in the mid to upper 70 s [53, 55]. Crystallinity is crucial for CNCs because the higher the crystallinity, the higher the stiffness they will impart on a polymer matrix during mechanical reinforcement [5, 56]. The p-CNCs showed a normal percent crystallinity compared to literature, which is suggested correlate to increased mechanical reinforcement properties. As well, each peak was separated and analyzed using the Scherrer equation with full width at half maximum (FWHM) to determine the size of each crystal plane, following an analysis by Kumar et al. and Das et al. [57, 58]. The resulting crystallite sizes were 8.6 nm, 5.7 nm, 3.4 nm, and 2.9 nm, for the 10$\bar{1}$, 021, 002, and 040 planes, respectively.
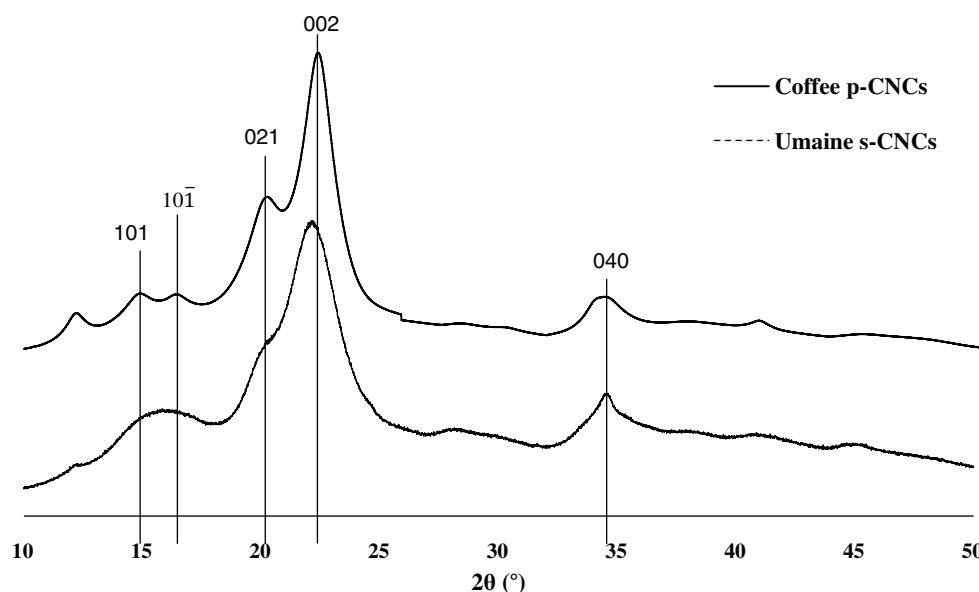

Figure 2: XRD spectra showing the crystalline peaks associated with the p-CNCs compared to those of commercial UMaine s-CNCs, with the 10$\bar{1}$, 021, 002, and 040 planes indicative of cellulose type I. The s-CNCs show an additional peak at the 101 plane which is associated with a higher crystallinity [55]

3.6 Thermal Stability - TGA

P-CNCs have been shown in literature to have an increased onset of thermal degradation when compared to other functionalized CNCs. This is believed to be caused by the instability of higher number of surface charges attributed to different functionalization, such as sulfate or carboxyl groups instead of phosphate groups [8, 49]. As surface charge increases or decreases, thermal stability responds oppositely, resulting in changing onsets of thermal degradation, i.e., 285°C and 330°C for s-CNCs and unmodified CNCs (h-CNCs), respectively [8]. It should be noted that h-CNCs possess only unmodified hydroxyl

groups produced from hydrolysis via hydrochloric acid. TGA of p-CNCs showed an onset of thermal degradation, measured at a loss of 5 wt% after the loss of humidity content ($T_{d5\%}$), of 310°C, shown in Fig. 3. This correlates well with other reported onsets of p-CNCs ranging from 290°C-330°C, sitting in between the higher and lower $T_{d5\%}$ of the s-CNCs and h-CNCs [8, 49, 56]. It should be noted that the $T_{d5\%}$ of each sample was shifted with respect to the humidity content of roughly 4 wt%, 6 wt%, and 3 wt% for the p-CNCs, s-CNCs, and h-CNCs, respectively. The difference in humidity content can be attributed to increasing water absorption by the CNCs as surface charge density increases [5-6]. Higher thermal stabilities have proven to be useful for multiple applications, such as casting and melt pressing films, and extrusion processing, without causing degradation or reduction of properties of the CNCs [14, 22, 59].
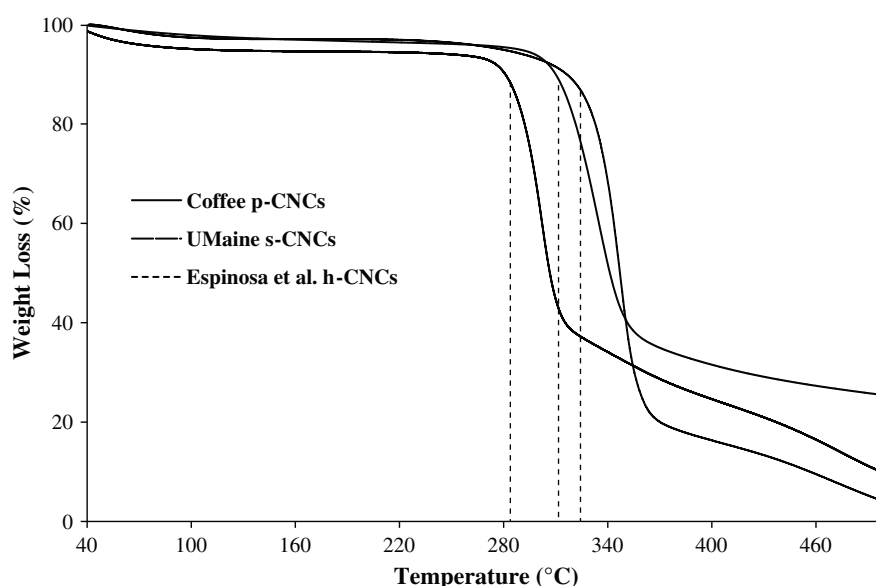

Figure 3: TGA plot comparing the thermal degradation of the isolated p-CNCs to commercially available s-CNCs. The vertical dotted lines refer to the onset of thermal degradation at $T_{d5\%} = 310°C$ for the p-CNCs and $T_{d5\%} = 285°C$ for the s-CNCs. These can also be compared to h-CNCs found in literature with an onset of $T_{d5\%} = 330°C$ [8]

3.7 Dispersibility and DLS

After initial sonication in the solvents, the p-CNCs showed good dispersion in water, DMSO, and DMF, while remaining agglomerated in THF. Continuing to monitor the dispersions, the p-CNCs did not show precipitation or agglomeration in either the water, DMSO, or DMF after a full ten days, as shown in Fig. 4. Furthermore, the p-CNCs dispersed in DMSO and DMF continued to improve over time, and showed no signs of precipitates or agglomerations after an extended time of over two months. The higher clarity within the DMSO and DMF suspensions show ideal dispersions with no precipitates or subsequent refraction of light [8, 43, 60, 61]. Therefore, it should be noted that although birefringence behaviors were not displayed using crossed nicols, the dispersability is still comparable to literature references for both with and without birefringence, in which precipitates can be seen in non-ideal solvents such as THF and partially for water [8, 43, 60-63]. A key factor of CNCs dispersion has to do with the amount of charge on the surface, and how well they repel each other and accept the solvent. As surface charge increases due to higher phosphate contents or different functionalization (i.e., sulfate groups or carboxyl groups), dispersion in solvents increases since repulsion between CNCs is greater [5, 6].
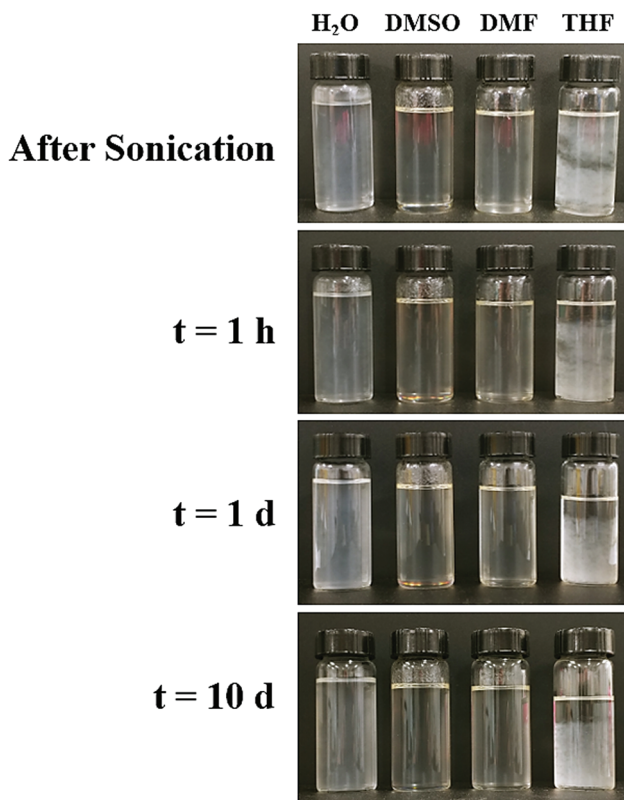
Figure 4: Images showing the 10 mg/mL p-CNC dispersions in water, DMSO, DMF, and THF, immediately following sonication, and subsequent times of 1 h, 1 d, and 10 d. The solvents used decrease in polarity from left to right

Further characterizing dispersibility of the p-CNCs, DLS was used to determine apparent particle size in a diluted DMF dispersion. DMF was chosen as the dispersant of choice due to overwhelming literature regarding CNC dispersion in DMF [8, 21]. DLS of the p-CNC suspension showed typical bimodal peaks with an apparent size of 139 nm-562 nm, which resides on the larger end of literature, with normal sizes ranging from 163 nm-250 nm for Vanderfleet et al. to upwards of 400 nm-500 nm for Shanmugarajah et al. [49, 64]. The larger size range can be attributed to the difficulty of perfectly redispersing dried p-CNCs into solvents, therefore retaining small aggregates within the suspension is possible and probable. The ability for CNCs to disperse readily in solvents is crucial for integrating them into polymer composites. Uniform dispersion in the polymer matrix creates ideal networks between CNCs and the matrix, allowing for isotropic behaviors while retaining little to no defects from CNC agglomeration [21].

3.8 Mechanical Reinforcement in Composites

The p-CNCs dispersed in the PU matrix showed a significant increase in mechanical properties compared to the neat PU, increasing the tensile modulus from (20.8 ± 0.8) MPa to (58.6 ± 2.7) MPa and increasing yield stress from (1.8 ± 0.1) MPa to (2.6 ± 0.1) MPa, respectively. However, the p-CNC composites showed lower mechanical properties when compared to commercial UMaine s-CNC composites, with a tensile modulus of (113.7 ± 9.7) MPa and yield stress of (3.6 ± 0.0) MPa, shown in Fig. 5. Although there was not as much of an increase in mechanical reinforcement with the p-CNCs as with the s-CNCs, significant reinforcement with regards to the pure polymer shows potential for use in many polymer composite applications. The ability of the p-CNCs to reinforce the polymer matrix is
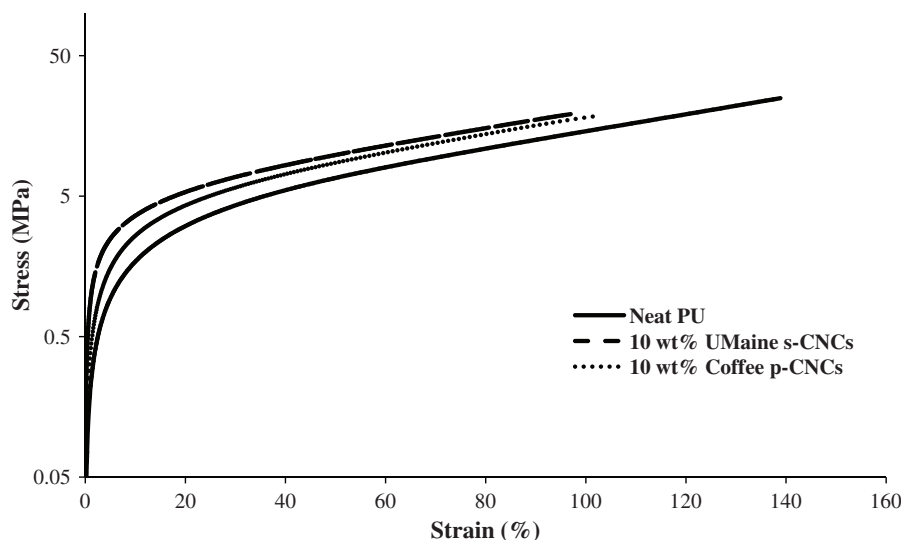
Figure 5: Tensile test results obtained with a DMA under controlled force ramp, showing a typical stress versus strain plot of neat PU, 10 wt% commercial UMaine s-CNCs in PU, and 10 wt% isolated p-CNCs in PU, to determine the reinforcement properties of the p-CNCs

crucial to the variety of applications of which it can be useful, such as strengthening a polymer for automotive industry compared to use in intervertebral disc or cartilage replacement [11, 12, 21, 44].

To avoid common misconception, it should be noted that although tension testing is typically run using controlled crosshead displacement or strain ramp on an Instron [65-67], stress versus strains curves, and subsequent tensile moduli, can be determined through controlled force ramps using a DMA [21, 43, 68, 69]. DMA uses an input of force while measuring the resultant strain, leading to an acceptable linear regime for tensile moduli analysis [21, 43, 68, 69].

These differences can be caused by many variables, however, the most probable are surface charge density, crystallinity, and aspect ratio. As discussed previously in *Section 3.7*, surface charge density has a drastic impact on the ability of CNCs to disperse in a solvent. P-CNCs show a lower dispersibility than commercial s-CNCs in common solvents, which can lead to a less uniform dispersion and more agglomerations within the polymer matrix [8]. A continuous network of CNCs and high number of CNC-polymer interactions are needed to create a mechanically robust composite. These problems can cause defects in the continuous CNC network, reducing the overall mechanical properties from lower CNC-polymer interactions [8]. As alluded in *Section 3.5*, crystallinity plays a major role in the reinforcement of a polymer matrix. The higher the crystallinity of the CNCs, the higher the stiffness and strength, which directly correlates to increased reinforcement [43, 52]. However, the p-CNCs produced in this study showed an around average crystallinity, therefore is assumed to not have had much impact on the decreased reinforcement. The final notable variable for the lower mechanical reinforcement is the aspect ratio of the p-CNCs compared to the commercial s-CNCs, most likely caused by the source of cellulose [11, 12]. The p-CNC aspect ratio of 12 ± 3, which were derived from spent coffee grounds, is on the lower end of the 10-40 aspect ratio range for the commercial s-CNC derived from wood pulp. As aspect ratio increases, the critical percolation threshold in the polymer composites decreases, resulting in less CNCs needed to create a continuous network and mechanically reinforce the polymer [12]. Therefore, at 10 wt% CNCs in PU, the commercial s-CNCs will have greater stress transfer between the CNCs and polymer matrix due to a larger, stiffer continuous network of CNCs [11, 12, 70]. However, it has been

shown that as long as the aspect ratio is at or above 10, significant reinforcement is achieved in most polymer composite systems, as proven by the p-CNCs in this study [12].

4 Conclusions

This study sought to establish a protocol for the isolation and characterization of p-CNCs from spent coffee grounds as a potential cellulosic waste material. The extraction of p-CNCs from the amorphous cellulose via phosphoric acid hydrolysis was proven successful, and further chemical and physical characterization determined the viability of the p-CNCs' usefulness. The resulting p-CNCs showed an aspect ratio of 12 ± 3, an apparent crystallinity of 74.2%, and a high phosphate content and surface charge density of (25.8 ± 9.6) mM/kg cellulose and (48.4 ± 6.2) mM/kg cellulose, respectively. The p-CNCs showed dispersibility in multiple organic solvents, with DMSO and DMF being the best candidates for dispersion. Nanocomposites were made using 10 wt% isolated coffee p-CNCs in PU and 10 wt% commercial UMaine s-CNCs in PU, and compared to determine the mechanical reinforcement ability in p-CNCs in a polymer-based nanocomposite. Although the nanocomposite reinforced with p-CNCs did not exhibit the same mechanical reinforcement as the commercial s-CNCs, there was still a three-fold increase in tensile modulus when compared to the neat PU. The dispersibility and mechanical reinforcement bodes well for the ability of the p-CNCs to be used in many polymer nanocomposite applications, in which fine tuning of p-CNC concentration is needed to achieve the necessary mechanical properties [11, 12, 21]. As well, the high phosphate content will increase the biocompatibility of the p-CNCs and cell adhesion and growth when introduced into a biocompatible polymer system [44]. The produced p-CNCs from spent coffee grounds compared well to other isolated CNCs from agricultural wastes throughout literature. Although the yield of CNCs was only about 8-10% of the starting raw material, the nearly limitless source of spent coffee grounds worldwide allows for potential mass quantities to be produced, regardless of low yield. With this in mind and the promise shown in this study, advancements toward industrial scalability should be further researched to determine the overall economic and environmental benefits of these results. Specifically, by the known sulfuric acid hydrolysis procedure already used in many industrial CNC manufacturers, such as University of Maine and Celluforce [50].

Conflict of Interest: The authors declare that they have no conflicts of interest to report regarding the present study.

References

1. Hon, D. N. S. (1994). Cellulose: a random walk along its historical path. *Cellulose, 1(1),* 1–25. DOI 10.1007/ BF00818796.

2. Holtzapple, M. T. (2003). Cellulose. In: Caballero, B., ed. *Encyclopedia of Food Sciences and Nutrition*. Second Edition. Academic Press: Oxford, 998–1007.

3. O'Sullivan, A. C. (1997). Cellulose: the structure slowly unravels. *Cellulose, 4(3),* 173–207. DOI 10.1023/ A:1018431705579.

4. Klemm, D., Heublein, B., Fink, H. P., Bohn, A. (2005). Cellulose: fascinating biopolymer and sustainable raw material. *Angewandte Chemie International Edition, 44(22),* 3358–3393. DOI 10.1002/anie.200460587.

5. George, J., Sabapathi, S. N. (2015). Cellulose nanocrystals: synthesis, functional properties, and applications. *Nanotechnology, Science and Applications, 8,* 45–54. DOI 10.2147/NSA.S64386.

6. Habibi, Y., Lucia, L. A., Rojas, O. J. (2010). Cellulose nanocrystals: chemistry, self-assembly, and applications. *Chemical Reviews, 110(6),* 3479–3500. DOI 10.1021/cr900339w.

7. Xing, L., Gu, J., Zhang, W., Tu, D., Hu, C. (2018). Cellulose I and II nanocrystals produced by sulfuric acid hydrolysis of Tetra pak cellulose I. *Carbohydrate Polymers, 192,* 184–192. DOI 10.1016/j.carbpol.2018.03.042.

8. Camarero Espinosa, S., Kuhnt, T., Foster, E. J., Weder, C. (2013). Isolation of thermally stable cellulose nanocrystals by phosphoric acid hydrolysis. *Biomacromolecules, 14(4),* 1223–1230. DOI 10.1021/bm400219u.

9. Foster, E. J., Moon, R. J., Agarwal, U. P., Bortner, M. J., Bras, J. et al. (2018). Current characterization methods for cellulose nanomaterials. *Chemical Society Reviews, 47(8),* 2609–2679. DOI 10.1039/C6CS00895J.

10. Moon, R. J., Martini, A., Nairn, J., Simonsen, J., Youngblood, J. (2011). Cellulose nanomaterials review: structure, properties, and nanocomposites. *Chemical Society Reviews, 40(7),* 3941–3994. DOI 10.1039/c0cs00108b.

11. Dufresne, A. (2012). *Nanocellulose: from nature to high performance tailored materials*. Berlin; Boston: De Gruyter.

12. Dufresne, A. (2013). Nanocellulose: a new ageless bionanomaterial. *Materials Today, 16(6),* 220–227. DOI 10.1016/j.mattod.2013.06.004.

13. Inc., F. M. (2019). The global market for nanocellulose to 2030. Technology Report 60.

14. Nicharat, A., Shirole, A., Foster, E. J., Weder, C. (2017). Thermally activated shape memory behavior of melt-mixed polyurethane/cellulose nanocrystal composites. *Journal of Applied Polymer Science, 134(27),* 45033. DOI 10.1002/app.45033.

15. Natterodt, J. C., Sapkota, J., Foster, E. J., Weder, C. (2017). Polymer nanocomposites with cellulose nanocrystals featuring adaptive surface groups. *Biomacromolecules, 18(2),* 517–525. DOI 10.1021/acs.biomac.6b01639.

16. Sapkota, J., Natterodt, J. C., Shirole, A., Foster, E. J., Weder, C. (2016). Fabrication and properties of polyethylene / cellulose nanocrystal composites. *Macromolecular Materials and Engineering, 302(1),* 1600300. DOI 10.1002/ mame.201600300.

17. Mendez, J., Annamalai, P. K., Eichhorn, S. J., Rusli, R., Rowan, S. J. et al. (2011). Bioinspired mechanically adaptive polymer nanocomposites with water-activated shape-memory effect. *Macromolecules, 44(17),* 6827–6835. DOI 10.1021/ma201502k.

18. Smyth, M., Fournier, C., Driemeier, C., Picart, C., Foster, E. J. et al. (2017). Tunable structural and mechanical properties in liquid of cellulose nanofiber substrates for stem cell culture. *Biomacromolecules, 18(7),* 2034–2044. DOI 10.1021/acs.biomac.7b00209.

19. Smyth, M., M'Bengue, M. S., Terrien, M., Picart, C., Bras, J. et al. (2018). The effect of hydration on the material and mechanical properties of cellulose nanocrystal-alginate composites. *Carbohydrate Polymers, 179,* 186–195. DOI 10.1016/j.carbpol.2017.09.002.

20. DiLoreto, E., Haque, E., Berman, A., Moon, R. J., Kalaitzidou, K. (2019). Freeze dried cellulose nanocrystal reinforced unsaturated polyester composites: challenges and potential. *Cellulose, 26(7),* 4391–4403. DOI 10.1007/s10570-019-02377-1.

21. Frost, B. A., Foster, E. J. (2019). Replication of annulus fibrosus through fabrication and characterization of polyurethane and cellulose nanocrystal composite scaffolds. *Nanocomposites, 5(1),* 13–27. DOI 10.1080/ 20550324.2019.1585651.

22. Venkantramen, P., Gohn, A. M., Rhoades, A. M., Foster, E. J. (2019). Developing high performance PA 11/ cellulose nanocomposites for industrial-scale melt processing. *Composites Part B-Engineering, 174,* 106988. DOI 10.1016/j.compositesb.2019.106988.

23. Tran, A., Hamad, W. Y., MacLachlan, M. J. (2018). Fabrication of cellulose nanocrystal films through differential evaporation for patterned coatings. *ACS Applied Nano Materials, 17(7),* 3098–3104. DOI 10.1021/ acsanm.8b00947.

24. Giese, M., Spengler, M. (2019). Cellulose nanocrystals in nanoarchitectonics – towards photonic functional materials. *Molecular Systems Design & Engineering, 4(1),* 29–48. DOI 10.1039/C8ME00065D.

25. Tingaut, P., Zimmermann, T., Sebe, G. (2012). Cellulose nanocrystals and microfibrillated cellulose as building blocks for the design of hierarchical functional materials. *Journal of Materials Chemistry, 22(38),* 20105–20111. DOI 10.1039/c2jm32956e.

26. Kuhnt, T., Herrmann, A., Benczédi, D., Foster, E. J., Weder, C. (2015). Functionalized cellulose nanocrystals as nanocarriers for sustained fragrance release. *Polymer Chemistry, 6(36),* 6553–6562. DOI 10.1039/C5PY00944H.

27. Schyrr, B., Pasche, S., Voirin, G., Weder, C., Simon, Y. C. et al. (2014). Biosensors based on porous cellulose nanocrystal – poly (vinyl alcohol) as scaffolds. *ACS Applied Materials & Interfaces, 6(15),* 12674–12683. DOI 10.1021/am502670u.

28. Potter, K. A., Jorfi, M., Householder, K. T., Foster, E. J., Weder, C. et al. (2014). Curcumin-releasing mechanically-adaptive intracortical implants improve the proximal neuronal density and blood-brain barrier stability. *Acta Biomaterialia, 10(5),* 2209–2222. DOI 10.1016/j.actbio.2014.01.018.

29. Jorfi, M., Roberts, M. N., Foster, E. J., Weder, C. (2013). Mechanically-adaptive bio-nanocomposites for biomedical applications. *ACS Applied Materials & Interfaces, 5(4),* 1517–1526. DOI 10.1021/am303160j.

30. Alexandrescu, L., Syverud, K., Nicosia, A., Santachiara, G., Fabrizi, A. et al. (2016). Airborne nanoparticles filtration by means of cellulose nanofibril based materials. *Journal of Biomaterials & Nanobiotechnology, 7,* 29–36. DOI 10.4236/jbnb.2016.71004.

31. Mussatto, S. I., Machado, E. M. S., Martins, S., Teixeira, J. A. (2011). Production, composition, and application of coffee and its industrial residues. *Food and Bioprocess Technology, 4(5),* 661–672. DOI 10.1007/s11947-011-0565-z.

32. Mussatto, S. I., Carneiro, L. M., Silva, J. P. A., Roberto, I. C., Teixeira, J. A. (2011). A study on chemical constituents and sugars extraction from spent coffee grounds. *Carbohydrate Polymers, 83(2),* 368–374. DOI 10.1016/j.carbpol.2010.07.063.

33. Woodward, J., Evans, B. (1996). Utilization of biocatalysts in cellulose waste minimization. *In Conference of Environmental Biomonitoring: The Biotechnology-Ecotoxicology Interface. United States Department of Energy (OSTI).* https://www.osti.gov/servlets/purl/374146.

34. Nagendran, R. (2011). Chapter 24 - Agricultural waste and pollution. In: Letcher, T. M., Vallero, D. A., eds. *Waste.* Boston: Academic Press, 341–355.

35. Wang, Y. (2010). Fiber and textile waste utilization. *Waste and Biomass Valorization, 1(1),* 135–143. DOI 10.1007/s12649-009-9005-y.

36. Silvério, H. A., Flauzino Neto, W. P., Dantas, N. O., Pasquini, D. (2013). Extraction and characterization of cellulose nanocrystals from corncob for application as reinforcing agent in nanocomposites. *Industrial Crops and Products, 44,* 427–436. DOI 10.1016/j.indcrop.2012.10.014.

37. Mendes, C. A. D. C., Ferreira, N. M. S., Furtado, C. R. G., de Sousa, A. M. F. (2015). Isolation and characterization of nanocrystalline cellulose from corn husk. *Materials Letters, 148,* 26–29. DOI 10.1016/j.matlet.2015.02.047.

38. Johar, N., Ahmad, I., Dufresne, A. (2012). Extraction, preparation and characterization of cellulose fibres and nanocrystals from rice husk. *Industrial Crops and Products, 37(1),* 93–99. DOI 10.1016/j.indcrop.2011.12.016.

39. Thambiraj, S., Shankaran, D. R. (2017). Preparation and physicochemical characterization of cellulose nanocrystals from industrial waste cotton. *Applied Surface Science, 412,* 405–416. DOI 10.1016/j.apsusc.2017.03.272.

40. Lam, N. T., Chollakup, R., Smitthipong, W., Nimchua, T., Sukyai, P. (2017). Characterization of cellulose nanocrystals extracted from sugarcane bagasse for potential biomedical materials. *Sugar Tech, 19(5),* 539–552. DOI 10.1007/s12355-016-0507-1.

41. Collazo-Bigliardi, S., Ortega-Toro, R., Chiralt Boix, A. (2018). Isolation and characterisation of microcrystalline cellulose and cellulose nanocrystals from coffee husk and comparative study with rice husk. *Carbohydrate Polymers, 191,* 205–215. DOI 10.1016/j.carbpol.2018.03.022.

42. Alghooneh, A., Mohammad Amini, A., Behrouzian, F., Razavi, S. M. A. (2017). Characterisation of cellulose from coffee silverskin. *International Journal of Food Properties, 20(11),* 2830–2843. DOI 10.1080/10942912.2016.1253097.

43. Marett, J., Aning, A., Foster, E. J. (2017). The isolation of cellulose nanocrystals from pistachio shells via acid hydrolysis. *Industrial Crops and Products, 109,* 869–874. DOI 10.1016/j.indcrop.2017.09.039.

44. Camarero-Espinosa, S., Rothern-Rutishauser, B., Weder, C., Foster, E. J. (2016). Directed cell growth in multi-zonal scaffolds for cartilage tissue engineering. *Biomaterials, 74,* 42–52. DOI 10.1016/j.biomaterials.2015.09.033.

45. Lokker, B. (2013). Coffee roasts from light to dark. *https://www.coffeecrossroads.com/coffee-101/coffee-roasts-from-light-to-dark*.

46. Ballesteros, L. F., Teixeira, J. A., Mussatto, S. I. (2014). Chemical, functional, and structural properties of spent coffee grounds and coffee silverskin. *Food and Bioprocess Technology, 7(12),* 3493–3503. DOI 10.1007/s11947-014-1349-z.

47. Mueller, S., Weder, C., Foster, E. J. (2014). Isolation of cellulose nanocrystals from pseudostems of banana plants. *RSC Advances, 4(2),* 907–915. DOI 10.1039/C3RA46390G.

48. Zhang, J., Wang, Y., Zhang, L., Zhang, R., Liu, G. et al. (2014). Understanding changes in cellulose crystalline structure of lignocellulosic biomass during ionic liquid pretreatment by XRD. *Bioresource Technology, 151,* 402–405. DOI 10.1016/j.biortech.2013.10.009.

49. Vanderfleet, O. M., Osorio, D. A., Cranston, E. D. (2018). Optimization of cellulose nanocrystal length and surface charge density through phosphoric acid hydrolysis. *Philosophical Transactions of the Royal Society A: Mathematical, Physical and Engineering Sciences, 376(2112),* 20170041. DOI 10.1098/rsta.2017.0041.

50. Reid, M. S., Villalobos, M., Cranston, E. D. (2017). Benchmarking cellulose nanocrystals: from the laboratory to industrial production. *Langmuir, 33(7),* 1583–1598. DOI 10.1021/acs.langmuir.6b03765.

51. Zhao, H., Kwak, J. H., Conrad Zhang, Z., Brown, H. M., Arey, B. W. et al. (2007). Studying cellulose fiber structure by SEM, XRD, NMR and acid hydrolysis. *Carbohydrate Polymers, 68(2),* 235–241. DOI 10.1016/j.carbpol.2006.12.013.

52. Zhou, Y. M., Fu, S. Y., Zheng, L. M., Zhan, H. Y. (2012). Effect of nanocellulose isolation techniques on the formation of reinforced poly (vinyl alcohol) nanocomposite films. *Express Polymer Letters, 6(10),* 794–804. DOI 10.3144/expresspolymlett.2012.85.

53. Aguayo, M. G., Fernández Pérez, A., Reyes, G., Oviedo, C., Gacitua, W. et al. (2018). Isolation and characterization of cellulose nanocrystals from rejected fibers originated in the kraft pulping process. *Polymers, 10(10),* 1145. DOI 10.3390/polym10101145.

54. Noguchi, Y., Homma, I., Matsubara, Y. (2017). Complete nanofibrillation of cellulose prepared by phosphorylation. *Cellulose, 24(3),* 1295–1305. DOI 10.1007/s10570-017-1191-3.

55. Cheng, G., Zhou, M., Wei, Y. J., Cheng, F., Zhu, P. X. (2019). Comparison of mechanical reinforcement effects of cellulose nanocrystal, cellulose nanofiber, and microfibrillated cellulose in starch composites. *Polymer Composites, 40(S1),* E365–E372. DOI 10.1002/pc.24685.

56. Jain, R. K., Lal, K., Bhatnagar, H. L. (1985). Thermal degradation of cellulose and its phosphorylated products in air and nitrogen. *Journal of Applied Polymer Science, 30(3),* 897–914. DOI 10.1002/app.1985.070300302.

57. Kumar, A., Negi, Y. S., Choudhary, V., Bhardwaj, N. K. (2014). Characterization of cellulose nanocrystals produced by acid-hydrolysis from sugarcane bagasse as agro-waste. *Journal of Materials Physics and Chemistry, 2(1),* 1–8.

58. Das, K., Ray, D., Bandyopadhyay, N. R., Sengupta, S. (2010). Study of the properties of microcrystalline cellulose particles from different renewable resources by XRD, FTIR, Nanoindentation, TGA and SEM. *Journal of Polymers and the Environment, 18(3),* 355–363. DOI 10.1007/s10924-010-0167-2.

59. Jia, C., Bian, H., Gao, T., Jiang, F., Kierzewski, I. M. et al. (2017). Thermally stable cellulose nanocrystals toward high-performance 2D and 3D nanostructures. *ACS Applied Materials & Interfaces, 9(34),* 28922–28929. DOI 10.1021/acsami.7b08760.

60. Viet, D., Beck-Candanedo, S., Gray, D. G. (2007). Dispersion of cellulose nanocrystals in polar organic solvents. *Cellulose, 14(2),* 109–113. DOI 10.1007/s10570-006-9093-9.

61. Araki, J., Wada, M., Kuga, S., Okano, T. (2000). Birefringent glassy phase of a cellulose microcrystal suspension. *Langmuir, 16(6),* 2413–2415. DOI 10.1021/la9911180.

62. Urena-Benavides, E. E., Ao, G., Davis, V. A., Kitchens, C. L. (2011). Rheology and phase behavior of lyotropic cellulose nanocrystal suspensions. *Macromolecules, 44(22),* 8990–8998. DOI 10.1021/ma201649f.

63. Bondeson, D., Mathew, A., Oksman, K. (2006). Optimization of the isolation of nanocrystals from microcrystalline cellulose by acid hydrolysis. *Cellulose, 13(2),* 171–180. DOI 10.1007/s10570-006-9061-4.

64. Shanmugarajah, B., Kiew, P. L., Chew, I. M. L., Choong, T. S. Y., Tan, K. W. (2015). Isolation of nanocrystalline cellulose (NCC) from palm oil empty fruit bunch (EFB): preliminary result on FTIR and DLS analysis. *Chemical Engineering Transactions, 45,* 1705–1710.

65. Bras, J., Viet, D., Bruzzese, C., Dufresne, A. (2011). Correlation between stiffness of sheets prepared from cellulose whiskers and nanoparticles dimensons. *Carbohydrate Polymers, 84(1),* 211–215. DOI 10.1016/j.carbpol.2010.11.022.

66. Wik, V. M., Aranguren, M. I., Mosiewicki, M. A. (2011). Castor oil-based polyurethanes containing cellulose nanocrystals. *Polymer Engineering and Science, 51(7),* 1389–1396. DOI 10.1002/pen.21939.

67. Liu, D., Zhong, T., Chang, P. R., Li, K., Wu, Q. (2010). Starch composites reinforced by bamboo cellulosic crystals. *Bioresource Technology, 101(7),* 2529–2536. DOI 10.1016/j.biortech.2009.11.058.

68. Ulbrich, R. R., Wadud, S. E. B. (2019). Dynamic mechanical analyzer DMA 2980. *http://www.tainstruments.com/pdf/literature/newdma.pdf*.

69. Menard, K. P. (2008). *Dynamic mechanical analysis: a practical introduction*. Second Edition. Location: CRC Press.

70. Shrestha, S., Montes, F., Schueneman, G. T., Snyder, J. F., Youngblood, J. P. (2018). Effects of aspect ratio and crystal orientation of cellulose nanocrystals on properties of poly (vinyl alcohol) composite fibers. *Composites Science and Technology, 167,* 482–488. DOI 10.1016/j.compscitech.2018.08.032.